THE ROLE OF TELOGENETIC INJECTION OF MAGMATICALLY DERIVED CO_2 IN THE FORMATION OF DAWSONITE FROM THE CASTILLO FORMATION, CHUBUT GROUP, PATAGONIA, ARGENTINA

Marcos COMERIO

*Instituto de Estudios Andinos "Don Pablo Groeber", Departamento de Ciencias Geológicas,
FCEN-UBA, 1428 Buenos Aires, Argentina
Centro de Tecnología de Recursos Minerales y Cerámica (CETMIC-CIC-CONICET),
C. C. 49, Manuel B. Gonnet (B1897ZCA), Argentina*

Martín E. MOROSI

*Centro de Tecnología de Recursos Minerales y Cerámica (CETMIC-CIC-CONICET),
C. C. 49, Manuel B. Gonnet (B1897ZCA), Argentina*

Maisa TUNIK

*Instituto de Investigación en Paleobiología y Geología, Sede Alto Valle, Universidad Nacional de Río Negro,
Isidro Lobo 516, General Roca, Argentina*

José M. PAREDES

*Departamento de Geología, Universidad Nacional de la Patagonia "San Juan Bosco" Ruta Provincial Nº 1 s/n, km.4 (9005),
Comodoro Rivadavia, Argentina*

Patricia E. ZALBA

*School of Geosciences, Monash University, Melbourne, Australia
Centro de Tecnología de Recursos Minerales y Cerámica (CETMIC-CIC-CONICET),
C. C. 49, Manuel B. Gonnet (B1897ZCA), Argentina*

ABSTRACT

We report the occurrence of dawsonite, $NaAlCO_3(OH)_2$, in volcaniclastic rocks of the Albian hydrocarbon reservoir Castillo Formation, Golfo San Jorge Basin, neighboring the Cañadón Asfalto Basin in Patagonia; this is the first known occurrence in Argentina. Dawsonite replaces crystals pseudomorphically, and can also be found as a cement together with other carbonates, which induced a loss in the porosity of the host rock. Previous studies reported incomplete chemical reactions which suggested that oligoclase and analcime were dawsonite precursors. In the present work we document either totally achieved or incomplete chemical reactions which led to the transformation of analcime into kaolinite and dawsonite into kaolinite, respectively. These facts allowed us to deduce that the transformation of analcime into kaolinite was *via* dawsonite, minerals formed during different stages under a telogenetic regime. Dawsonite values of $\delta^{13}C$ PDB (–0.1 to 1.5‰) are consistent with a magmatic source of CO_2 provided by hypabyssal, basic alkaline igneous rocks of regional importance starting in the Eocene. We identify both internal and external sources of Na and Al used in the formation of dawsonite.

Keywords: Dawsonite, volcaniclastic rocks, magmatic CO_2, telogenesis, Patagonia, Argentina

§ *Corresponding author e-mail*: pezalba@cetmic.unlp.edu.ar; pezalba@yahoo.com.ar

INTRODUCTION

Dawsonite, $NaAlCO_3(OH)_2$, is prominent in exposures of the Castillo Formation, one of the main hydrocarbon reservoir units in the subsurface of the Golfo San Jorge Basin in Patagonia, Argentina. There, it was first reported in volcaniclastic rocks of the Cerro Castaño Member, Cerro Barcino Formation of the Chubut Group in the neighboring Cañadón Asfalto Basin. On that occasion Zalba *et al.* (2011) demonstrated: (1) that the occurrence of dawsonite was independent of textural control, occurring both in vitric tuffs and litharenites; (2) the existence of an inverse relationship between analcime and dawsonite attributed to an incomplete chemical reaction regarding these two minerals, together with (3) the transformation of oligoclase into dawsonite; and, consequently, (4) that analcime and oligoclase were dawsonite precursors.

Previous studies have demonstrated that dawsonite may be diagenetic in origin (Smith & Milton 1966, Goldbery & Loughnan 1977, Baker *et al.* 1995, Worden 2006, Liu *et al.* 2011), yet it can be hydrothermal in origin (Stevenson & Stevenson 1977, 1978, Ferrini *et al.* 2003), and may also be a weathering product in soils (Hay 1963, 1964).

It is important to highlight that in volcaniclastic rocks analcime has been reported as the precursor of dawsonite (Brobst & Tucker 1974, Mason 1983), whereas in sandstones feldspars are invoked as their parental minerals (*e.g.*, Baker *et al.* 1995, Worden 2006). In many units of the volcaniclastic Chubut Group several authors have attested to important occurrences of analcime, clinoptilolite or clinoptilolite-heulandite, and laumontite (Teruggi 1962, Iñíguez Rodríguez *et al.* 1987, Manassero *et al.* 2000, Zalba & Andreis 2003, Cladera *et al.* 2004, Tunik *et al.* 2004).

In this study we document new evidence regarding the occurrence of dawsonite and mineral replacements: (1) kaolinite pseudomorphs after analcime; (2) incipient, partial, and total replacement of dawsonite by kaolinite; (3) different steps in the replacement of plagioclase and also of alkali feldspar by dawsonite; (4) we explain why there is no textural control on the occurrence of dawsonite; and (5) we test the hypothesis that analcime and feldspar minerals, even if they are not found at present in the host volcaniclastic rocks, were necessary as internal sources of Na and Al, in addition to external Na, Al, and CO_2, for the formation of dawsonite.

Analcime and plagioclase, which characterize the Castillo Formation in other areas of the Golfo San Jorge Basin, have never previously been found associated with dawsonite in these rocks. We analyzed the occurrence of dawsonite-bearing volcaniclastic rocks and the syndepositional environment for the formation of its precursors. Also, the paragenetic association and the origin of dawsonite are discussed.

GEOLOGICAL BACKGROUND

The Golfo San Jorge Basin (Fig. 1a) is predominantly extensional and formed in response to the break-up of the Gondwana supercontinent during Jurassic and early Cretaceous time (Barcat *et al.* 1989). The Chubut Group (Barremian to Campanian? up to 7000 m thick, according to Fitzgerald *et al.* 1990) represents the incorporation of large volumes of volcaniclastic rocks in the basin related to the Cordillera de los Andes uplift. It is integrated by lacustrine rocks of the Pozo D-129 Formation (Barremian to Aptian), the main source rock of the basin, which grades laterally into the fluvial Matasiete Formation (Sciutto 1981, Paredes *et al.* 2007). Both units are covered by the Castillo Formation (Albian; Lesta & Ferello 1972), which in turn is overlain by the fluvial Bajo Barreal Formation (Cenomanian to Campanian? Sciutto 1981, Umazano *et al.* 2008). Towards the basin margin, the Bajo Barreal Formation grades to the Laguna Palacios Formation (Sciutto 1981, Genise *et al.* 2002).

Magmatic activity, with the development of extensive alkaline basaltic lavas and alkaline-basic intrusive bodies, occurred in the Late Eocene-Pleistocene (Bruni *et al.* 2008). At Sierra San Bernardo, tuffs and tuffaceous sandstones of the Castillo Formation were intruded by alkaline melts (Fernández Gianotti 1969). Menegatti *et al.* (2013) carried out a detailed petrographic study of these intrusives where plagioclase, alkali feldspar, and scarce nepheline are altered to analcime, and where alkali feldspar minerals may be altered to kaolinite.

The burial and thermal history of the Chubut Group has been reconstructed for different areas of the Golfo San Jorge Basin using maturity data (vitrinite reflectance) and corrected bottom hold temperatures derived from more than 1700 well logs. For different areas of the basin the burial depth achieved at the base of the Chubut Group was around 3000 m. If the average geothermal gradient for the whole basin is considered (3.55 °C/100 m), the base of the group attained temperatures above 100 °C (Sylwan *et al.* 2008).

The Castillo Formation: Previous studies

The Castillo Formation (Lesta & Ferello 1972) is broadly equivalent to the Cerro Castaño Member of the Cerro Barcino Formation (Lesta & Ferello 1972) in the Cañadón Asfalto Basin (Fitzgerald *et al.* 1990).

FIG. 1. (a) Location map of the Golfo San Jorge Basin. (b) Satellite image of the Sierra Silva anticline. (c) Overview of the study area showing outcrops of the Cretaceous units. (d) The stratigraphic column analyzed and samples collected from the Castillo Formation.
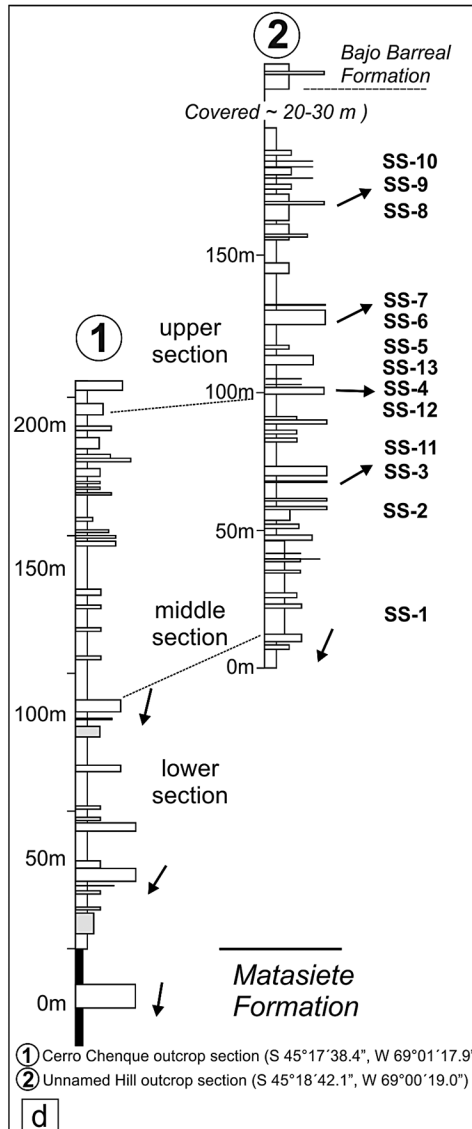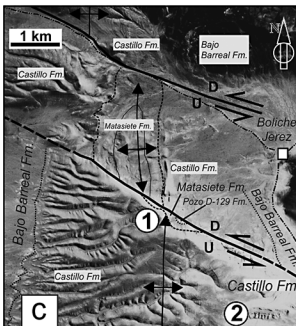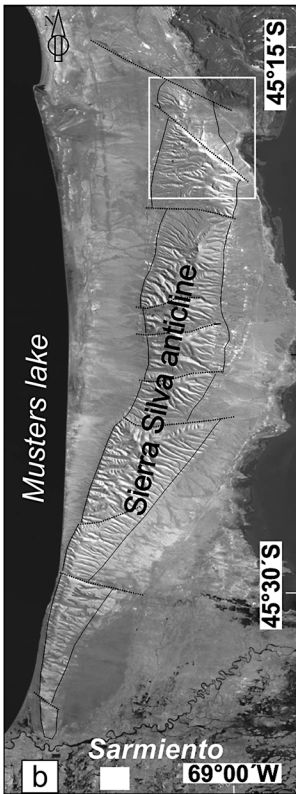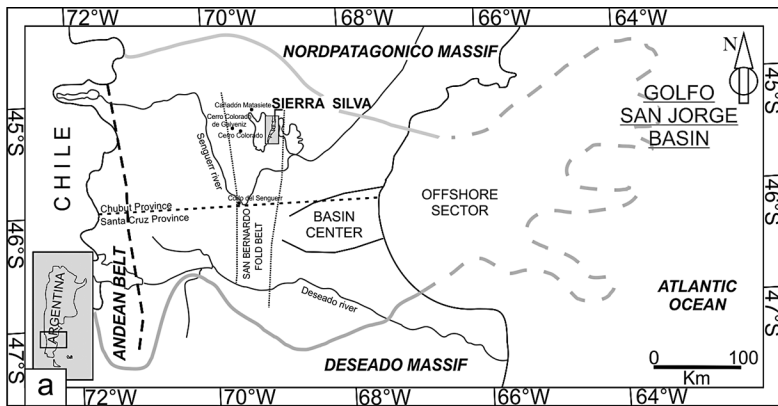
Tuff layers and ignimbrites intercalated in the Castillo Formation yielded Ar-Ar ages ranging from 104.8 to 94.2 Ma (Bridge *et al.* 2000). The unit as a whole is 2,200 m thick in the subsurface of the basin (Fitzgerald *et al.* 1990); in outcrops of the San Bernardo Fold Belt it thins northward from 964 m to around 30 m. In this area, Sciutto (1981) recognized a lower section which consists of tuff beds with minor epiclastic material and an upper section composed of tuff beds and sandstone bodies. Hechem *et al.* (1990) interpreted the lower section as lacustrine and the upper section as deposited by meandering fluvial systems.

In the San Bernardo Fold Belt petrographic contributions were made for diverse localities where the Castillo Formation outcrops (Fig. 1a). Teruggi (1962) and Teruggi & Rosetto (1963) described analcime for the first time in Argentina, in the Río Senguerr anticline area. Authigenic montmorillonite and analcime were found replacing pyroclastic and lithic fragments in lacustrine paleoenvironments. In the studied section, the crystalline fragments, in tuffs and tuffites, are dominated by plagioclase (andesine-oligoclase). This was also observed at Sierra de Castillo by Zalba & Andreis (2003), who remarked that the abundance of authigenic analcime revealed pyroclastic material deposited in extensive brackish lakes in a semiarid climate, attributing its formation to syndiagentic conditions. Tunik *et al.* (2004) carried out the first analysis concerning the source of lithic feldarenites at localities near the Sierra Silva anticline. As in previous studies, the authors stated that plagioclase is the most abundant crystalline component, and it is accompanied by analcime, chlorite, and kaolinite as cements.

SAMPLES AND METHODS

An integrated stratigraphic column of the Castillo Formation was analyzed along the north-eastern flank of the Sierra Silva anticline where middle and upper informal units have been recognized and systematically sampled (Figs. 1b, c, d). Dawsonite-bearing volcaniclastic rocks were studied by optical and electron microscopy as well as by X-ray diffraction and carbon-oxygen isotopic analysis. In addition, one sample of the lower section, important for our discussion, was powdered and X-rayed because it is representative of the typical mineralogy of the study unit in other areas.

Petrographic modal analyses were carried out and quantified by counting 300 points per slide. The samples were impregnated with a blue epoxy resin to highlight the porosity and with Alizarin Red S to identify carbonate minerals (Dickson 1965). The texture and mineralogical composition of the rocks were examined using a JEOL SEM/EDX.

X-ray diffraction (XRD) was carried out with a Philips 3020 instrument (Ni-filtered $CuK\alpha$, 35 kV, 40 mA, without secondary monochromator). For non-oriented samples step-scan data were obtained from 3 to 70° 2θ, with a step width of 0.04° and a counting time of 2s/step. Oriented samples (<2 μm) were prepared (air dried, glycolated overnight, and heated for 2 hours at 550 °C) for analysis of clay minerals. Mineral phases were analyzed and quantified with the FULLPROF program (Rodríguez Carvajal 2001), which is a multi-purpose profile-fitting standardless program which incorporates Rietveld refinement (Rietveld 1969).

Dawsonite-bearing samples were examined for their $\delta^{13}C$ and $\delta^{18}O$ isotopic values at the Instituto de Geocronología y Geología Isotópica (INGEIS), including duplicate and triplicate analyses. Carbonate minerals constitute more than 10% of the whole rock. The technique was based on the method developed by McCrea (1950). The CO_2 fraction was extracted by reaction with phosphoric acid at 60 °C over two hours, then was purified in a high-vacuum line, and analyzed with a mass spectrometer (Delta S Finnigan Mat triple collector). The $\delta^{13}C$ and $\delta^{18}O$ values were reported in ‰ relative to the standard V-PDB (Vienna Pee Dee Belemnitella, Coplen 1994) and to V-SMOW (Vienna Standard Mean Ocean Water), respectively. The analytical error was 0.1‰ (±2σ) for $\delta^{13}C$ and $\delta^{18}O$.

RESULTS

Stratigraphic section

A 280 m thick section of the Castillo Formation, whose top is eroded, overlies red mudstones of the Matasiete Formation (Sciutto 1981, Paredes *et al.* 2007) (Figs. 1c, d). The unit was informally subdivided into a lower, middle, and an upper section due to differences in the depositional framework. The lower section, 93 m thick, is dominated by floodplain deposits with large-scale, low-sinuosity fluvial sand bodies. The middle section, 97 m thick, is composed of very shallow, thinly laminated lacustrine and floodplain deposits. Finally, the upper section, 90 m thick, is characterized not only by low-to-moderate sinuosity fluvial channels, but also by floodplain deposits (Paredes 2009).

Petrographic description

Volcaniclastic sedimentary rocks. Lithological types were classified on the triangular diagram of Folk *et al.* (1970) as litharenites (Fig. 2a, Table 1). The matrix, which is partially to totally devitrified, consists of volcaniclastic fragments (<15 μm in size). Reworked pyroclastic fragments make up almost 25% of the rock on average. Completely altered glass shards and deformed pumice fragments were differentiated (Figs. 3a, b, c, d). Lithic fragments (40% on average and 0.5–1 mm in size) are felsic lava with felsitic, hyaloplitic, and pilotaxitic textures, and are completely to partially altered, highly rounded tuff fragments (Figs. 3d, e).

The remaining lithic fragments (<5% on average) are represented by polycrystalline quartz and sedimentary and plutonic/metamorphic rocks. The crystalline population (25% on average) is dominated by quartz, but also includes alkali feldspar and plagioclase. The quartz fragments are subhedral, angulose, and, in some cases, embayed and with normal extinction (Fig. 4a). Feldspar minerals may show significant alteration features and are partially to completely replaced by secondary minerals, sometimes only recognizable by their prismatic habit as well as by their cleavage and twinning relicts (Figs. 4a, b, c, d). However, oligoclase with albite twinning and alkali feldspar with corroded features have been distinguished (Figs. 4e, f). Intragranular porosity represents 5% on average of the whole rock (Fig. 4e).

Pyroclastic rocks. Following Gillespie & Styles (1999) the pyroclastic rocks, which contain more than 75% by volume of pyroclastic fragments, are classified as vitric tuffs on the Fisher & Schmincke (1984a) diagram (Fig. 2b, Table 1). Colorless glass shards, with planar and cuspate shapes which result in the typical X and Y forms, are the predominant components (80% on average and <100 μm in size). Pumice fragments (10% on average) are the largest ones (300 μm), and show canaliculi and, sometimes, corroded features. In the vitric tuffs, glass shards and pumice fragments are totally replaced by a submicroscopic crystalline aggregate (Fig. 3f). The crystalline and lithic (5% on average) components are similar to those already described for litharenites. Intragranular porosity represents less than 5% of the whole rock (Fig. 3f). Pyroclastic fragments are immersed in a mesostasis (30% by volume) completely altered to a submicroscopic crystalline aggregate (Fig. 3f) which shows a diffuse orientation (Fig. 3g).

X-ray diffraction (XRD)

Mineral phases in litharenites and vitric tuffs were identified using XRD of whole rock powder samples, including one sample of the lower section (Figs. 5a, b). Applying the Rietveld method (Rietveld 1969) it was possible to quantify mineral phases (Table 2). The *R*wp values (the weighted profile residual factor from refinement between observed and calculated patterns), which range from 14.5 to 28.7, are typical for XRD refinements according to Bish & Post (1993). Table 2 shows that in the litharenites quartz (50% on average) and kaolinite (20% on average) are the most abundant minerals. Dawsonite attains values of 10% on average. It was possible to identify both alkali and calco-sodic feldspars (less than 10% on average) where the former predominate over the latter. Calcite and ferroan dolomite are minor components. In vitric tuffs the association of quartz and kaolinite attains approximately 90% of the volume (Table 2 and Fig. 3f).

Scanning electron microscopy (SEM)

Mineral descriptions were made from the litharenites because in the vitric tuffs kaolinite and microcrystalline quartz have almost completely replaced the volcaniclastic components and the mesostasis.

Kaolinite plates completely replacing faces of analcime cube-octahedrons (Fig. 6a) were identified by SEM/EDX. The replacement of feldspar by dawsonite is documented by optical and SEM observations. Dawsonite fibers grow parallel to cleavage (probably 001) in albite-twinned crystals with (010) as the twin plane, and parallel to the [001] twin axis in Carlsbad-twinned crystals, at the expense of plagioclase and alkali feldspar, respectively. This suggests that the alteration was controlled by the structure of the primary
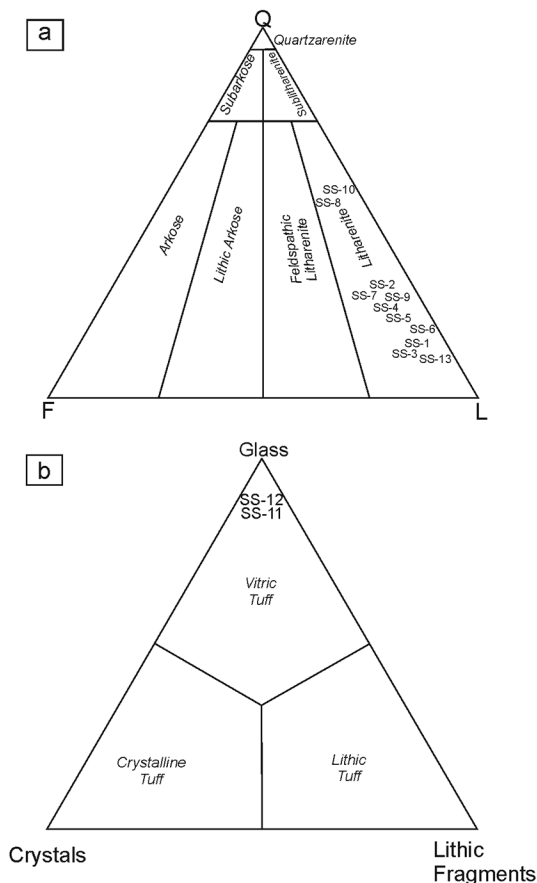

FIG. 2. (a) Sandstone classification diagram (Folk *et al.* 1970) for dawsonite-bearing rocks. (b) Triangular diagram intended for the classification of tuffs (Pettijohn *et al.* 1987).

TABLE 1. COMPOSITION OF VOLCANICLASTIC ROCKS OF THE CASTILLO FORMATION

SAMPLE	Qtzm (%)	Qtzp (%)	Pl (%)	Kfs (%)	Lv (%)	Lpir (%)	Lp/m (%)	Lsed (%)	Glass shards (%)	Pumice Fragments (%)	Op (%)	Θ (%)
SS-10	39	1	3	3	15	14	2		10	8	4	1
SS-9	20	2	1	5	20	9			5	31	2	5
SS-8	35		3	5	25	14			2	3	7	6
SS-7	21	2	4	6	38	12			3	1	8	5
SS-6	15		2	3	10	12			10	40	3	5
SS-5	16	1	2	4	29	10			8	23	1	6
SS-13	7		1	2	35	16			22	9	4	4
SS-4	20		5	2	26	13		2	18	5	5	4
SS-12	2		2	1		7			72	9	4	3
SS-11	5		1	3		6			76	3	5	1
SS-3	10		4	6	40	15			17	4	1	3
SS-2	23		3	5	35	10			4	11	5	4
SS-1	14	1	2	6	37	15			5	5	6	9

Qtzm: monocrystalline quartz, Qtzp: polycrystalline quartz, Pl: plagioclase, Kfs: K-feldspar, Lv: volcanic lithic, Lpir: pyroclastic lithic, Lp/m: plutonic/metamorphic lithic, Lsed: sedimentary lithic, Op: opaque minerals, Θ: porosity.

feldspars, as was observed in the incipient replacement of plagioclase (Figs. 4b, 6b, c) and of alkali feldspar (Figs. 4c, d) by dawsonite. In addition, it was possible to observe partially dissolved feldspar crystals with corroded features (Fig. 6d). Dawsonite fibers range from 1 to 10 μm wide and 50 to 100 μm long. Quartz occurs as pyramidal microcrystalline crystals (Fig. 6e). Stacks of pseudo-hexagonal kaolinite plates grow over dawsonite fibers (Fig. 6f).

Authigenic minerals in litharenites and vitric tuffs

Both rock types have been affected by dissolution, generation of intragranular porosity, replacement of primary minerals, and infilling of secondary pores and fissures. Authigenic minerals are represented by analcime, dawsonite (only in litharenites at present) and kaolinite, quartz, pyrite/hematite, calcite, and Fe-dolomite in both litharenites and vitric tuffs.

Analcime has been pseudomorphically replaced by kaolinite as documented in Figure 6a. Dawsonite constitutes, in some cases, an abundant component, reaching about 20% of the total volume of the rock (Table 2). The dawsonite appears as acicular crystals forming bundles and rosettes when growing from a common center and radiates outwards, increasing in size and forming large sheet-like aggregates (Figs. 7a, b). It occurs as: (1) partial replacement of twinned feldspars (Figs. 4c, d, 6c) and as pseudomorph after feldspars (Figs. 4a, b, 7a, b); (2) completely and partially replacing vitroclasts (Fig. 3c) and lithic fragments (Fig. 3e); and (3) as cement filling pore space among detrital grains, sometimes as spherulites (Figs. 4e, f, 7c). It is worth noting that dawsonite may be pseudomorphically replaced by pseudo-hexagonal plates of kaolinite (Fig. 6g and detail) and that the dawsonite fibers were never crushed.

In the litharenites, vitric (Figs. 3a, b) and lithic fragments, feldspar minerals (Figs. 4c, d), and the matrix (Figs. 6e, 7d) are, at present, composed of kaolinite and microcrystalline pyramidal quartz. Scanning electron microscopy observation shows that kaolinite occurs in the following forms: (1) as individual pseudo-hexagonal crystals with grain sizes of about 4 μm (Fig. 6c) and (2) as stacks of euhedral plates with vermiform habits (Fig. 6e).

In the vitric tuffs, glass shards, pumice fragments, as well as the mesostasis, are also composed of kaolinite and microcrystalline quartz (Fig. 3f).

Hematite cement occurs as a fringe around grains (Fig. 7a), fills cavities, and results mainly from the dissolution of volcaniclastic fragments (Figs. 4e, f). Hematite is also present as coatings on the walls of cracks and fissures, in some cases accompanied by kaolinite. Pyrite cement constitutes a minor component and it occurs as euhedral-cubic grains (10–15 μm) identified by optical microscopy. Reddened pyrite crystals suggest their oxidation to hematite. Euhedral hexagonal hematite crystals and irregular patches are distributed among volcaniclastic fragments in both litharenites and vitric tuffs, and over spherulitic dawsonite (Fig. 7c).

Besides dawsonite, other carbonates act as cement and/or as replacement minerals. The observation of stained thin sections confirmed the presence of both ferroan calcite and ferroan dolomite, represented by microspar and macrospar calcite (Figs. 7a, b, d, e, f, g) and by dolomicrite (Figs. 7f, g). Calcite partly dissolves dawsonite fibers in both cavities (Figs. 7a, b) and in the interior of crystals (Fig. 7f), and it also occurs as a pseudomorph after dawsonite (Fig. 7e), after feldspar minerals (Fig. 7g), as well as filling microcracks (Fig. 7d). Anhedral Fe-dolomite crystals (<16 μm) commonly occur around calcite cement (Fig. 7f).
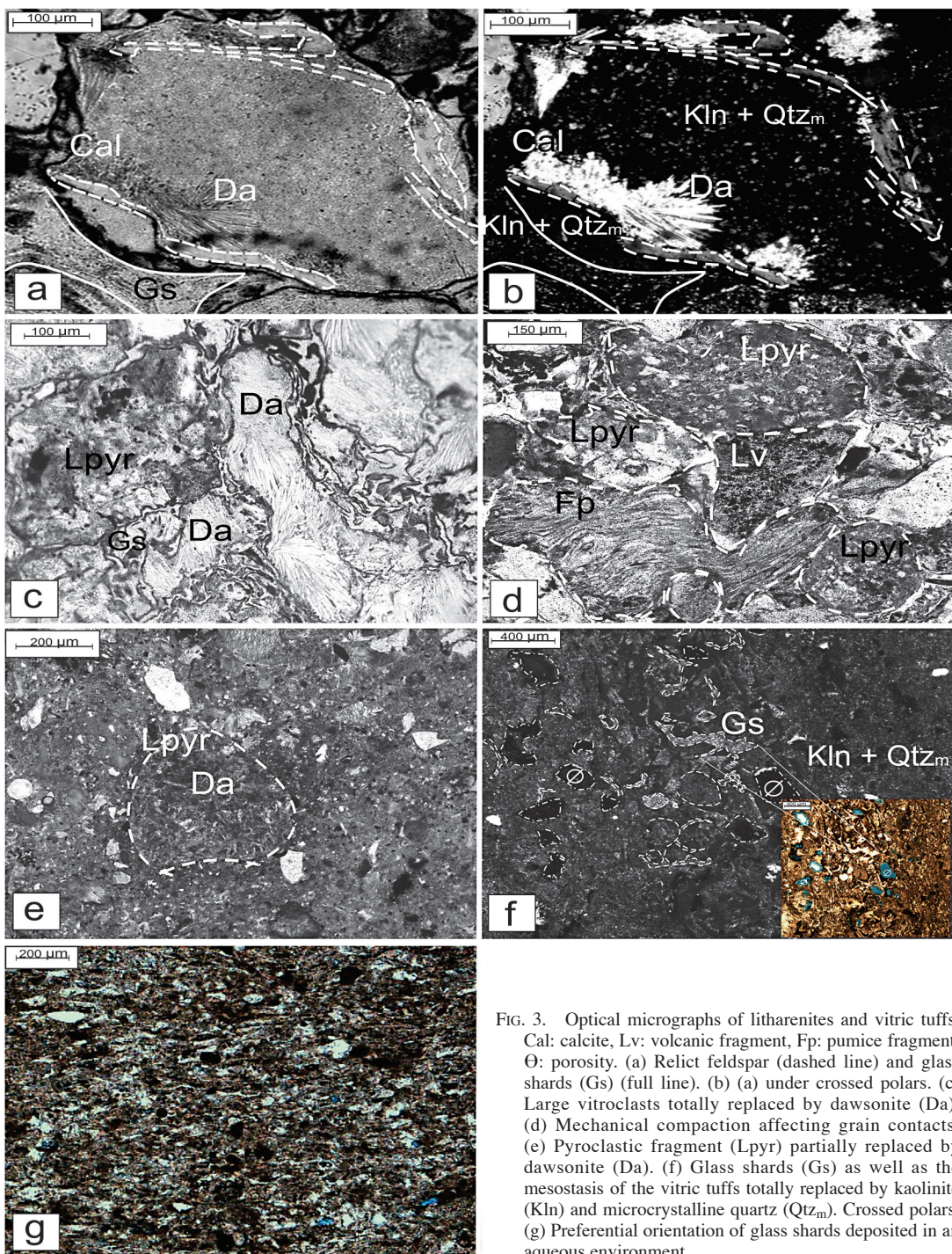
FIG. 3. Optical micrographs of litharenites and vitric tuffs. Cal: calcite, Lv: volcanic fragment, Fp: pumice fragment, Θ: porosity. (a) Relict feldspar (dashed line) and glass shards (Gs) (full line). (b) (a) under crossed polars. (c) Large vitroclasts totally replaced by dawsonite (Da). (d) Mechanical compaction affecting grain contacts. (e) Pyroclastic fragment (Lpyr) partially replaced by dawsonite (Da). (f) Glass shards (Gs) as well as the mesostasis of the vitric tuffs totally replaced by kaolinite (Kln) and microcrystalline quartz (Qtz_m). Crossed polars. (g) Preferential orientation of glass shards deposited in an aqueous environment.
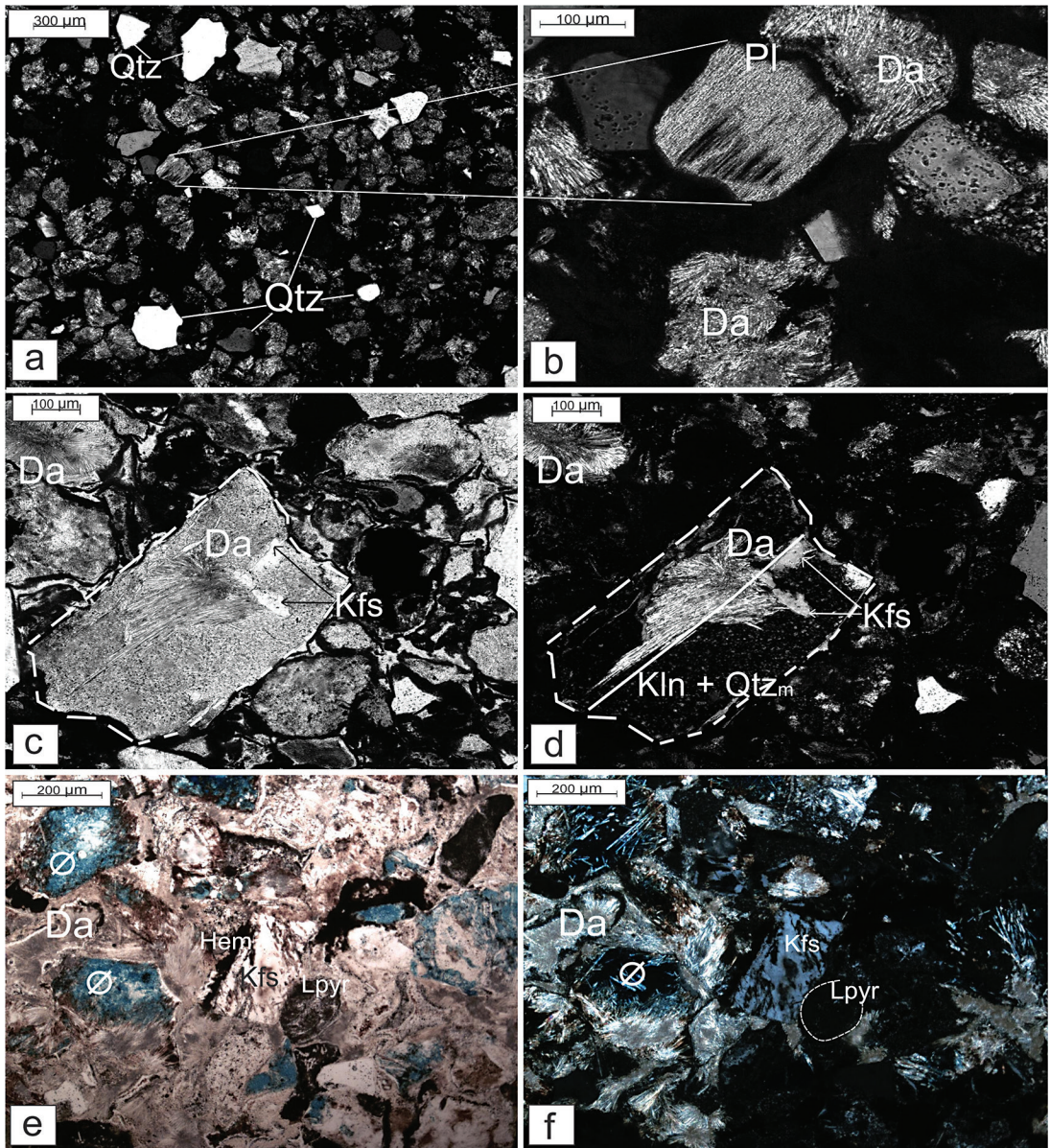
FIG. 4. Litharenites. Optical micrographs of feldspar population. Qtz: detrital quartz, Hem: hematite, Lpyr: pyroclastic fragment, Ɵ: porosity. (a) Dawsonite (Da) pseudomorph after feldspar minerals under crossed polars. (b) Detail of (a): incipient replacement of twinned plagioclase (Pl) by dawsonite (Da). (c) Dawsonite (Da) and kaolinite (Kln)-microcrystalline quartz (Qtz$_m$) after alkali feldspar (Kfs). (d) (c) under crossed polars. (e) Partially dissolved alkali feldspar (Kfs) and dawsonite (Da) cement filling pores. (f) (e) under crossed polars.

Stable isotope data

The $\delta^{13}C$ and $\delta^{18}O$ stable isotope analyses of the dawsonite-bearing litharenites were performed in duplicate and triplicate with consistent results, which are plotted in Figure 8. The fact that for samples SS-1, SS-8, and SS-10 dawsonite represents about 85% of the carbonate minerals indicates that $\delta^{13}C$‰ VPDB (–0.1, 0.7, and 1.5) and $\delta^{18}O$‰VsSMOW (15.7, 20.3, and 20.9) values represent its isotopic signature.

TABLE 2. QUANTITATIVE XRD ANALYSIS (WT.%) ON WHOLE ROCK SAMPLES (RIETVELD METHOD)

SAMPLE	dawsonite	kaolinite	calcite	Fe-dolomite	anatase	quartz	K-feldspar	plagioclase
SS-10	27.13(1.26)	21.42(1.88)	1.48(0.32)	1.61(0.37)	2.93(0.36)	34.30(1.23)	5.98(0.69)	5.15(0.78)
SS-8	10.87(1.09)	18.64(1.20)	1.10(0.30)	1.12(0.41)	1.80(0.30)	55.39(1.31)	5.99(0.65)	5.09(0.65)
SS-7	0.81(0.33)	20.14(0.78)	2.98(0.25)	1.44(0.28)	1.69(0.42)	56.93(0.95)	8.79(0.64)	7.22(0.39)
SS-6	4.99(0.24)	15.98(1.20)	0.76(0.21)	4.95(0.29)	1.03(0.02)	69.06(1.28)	2.19(0.77)	1.04(0.53)
SS-5	19.73(1.03)	13.11(0.86)	1.27(0.22)	7.64(0.41)	1.28(0.30)	46.71(1.33)	2.47(0.55)	7.79(0.97)
SS-13	3.76(0.18)	21.36(0.31)	0.36(0.10)	0.28(0.05)	0.60(0.10)	69.97(0.62)	2.54(0.15)	1.13(0.20)
SS-4	17.97(0.93)	9.95(0.45)	0.92(1.20)	24.42 (1.25)	1.57(0.37)	31.53(1.09)	5.74(0.85)	7.90(0.96)
SS-11	-	25.97(2.38)	0.45(0.29)	0.92(0.33)	1.82(0.66)	65.99(2.49)	1.38(0.78)	3.47(1.22)
SS-3	5.63(0.40)	11.42(0.82)	23.18(0.75)	1.20(0.22)	1.63(0.25)	40.98(0.85)	8.91(0.21)	7.05(0.33)
SS-2	1.70(0.99)	26.10(1.57)	1.05(0.50)	0.99(0.30)	1.10(0.47)	57.42(1.48)	7.42(0.60)	4.22(0.55)
SS-1	20.74(1.45)	19.87(1.43)	1.14(0.29)	1.35(0.35)	2.61(0.35)	40.86(1.69)	9.55(1.25)	3.88(0.75)

Estimated standard deviations were systematically corrected with Bérar and Lelann σ$_{corr}$ factor (Bérar & Lelann 1991).
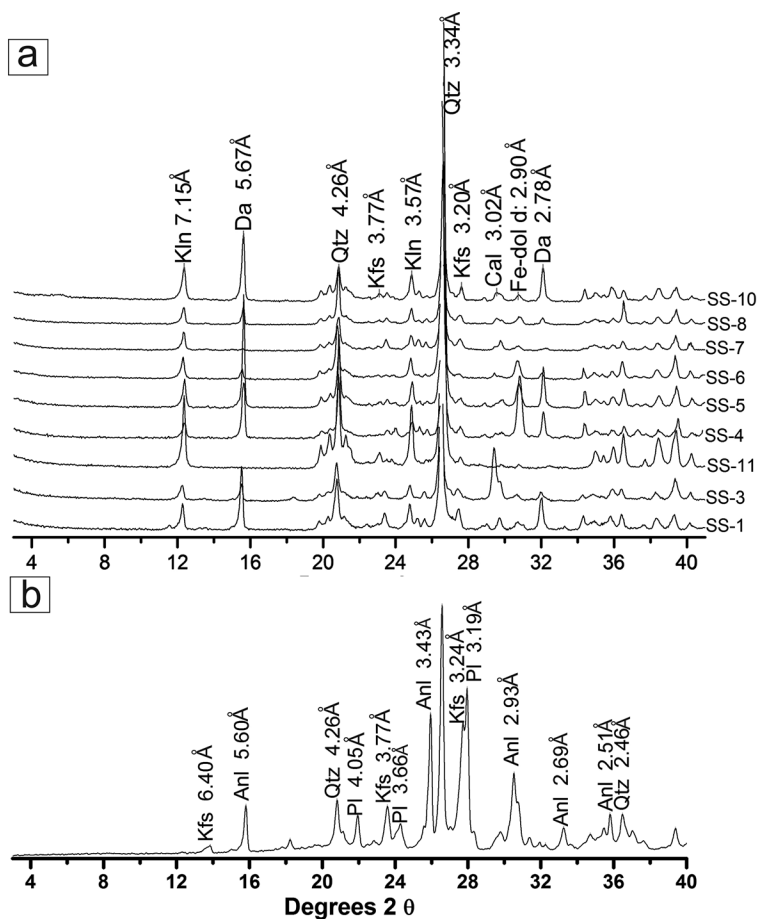

FIG. 5.   Anl: analcime, Cal: calcite, Da: dawsonite, Fe-Dol: ferroan dolomite, Kln: kaolinite, Kfs: K-feldspar, Pl: plagioclase, Qtz: quartz. (a) XRD of whole rock samples (middle and upper sections). (b) Diffraction pattern of a sample obtained from the lower section of the Cerro Chenque area.
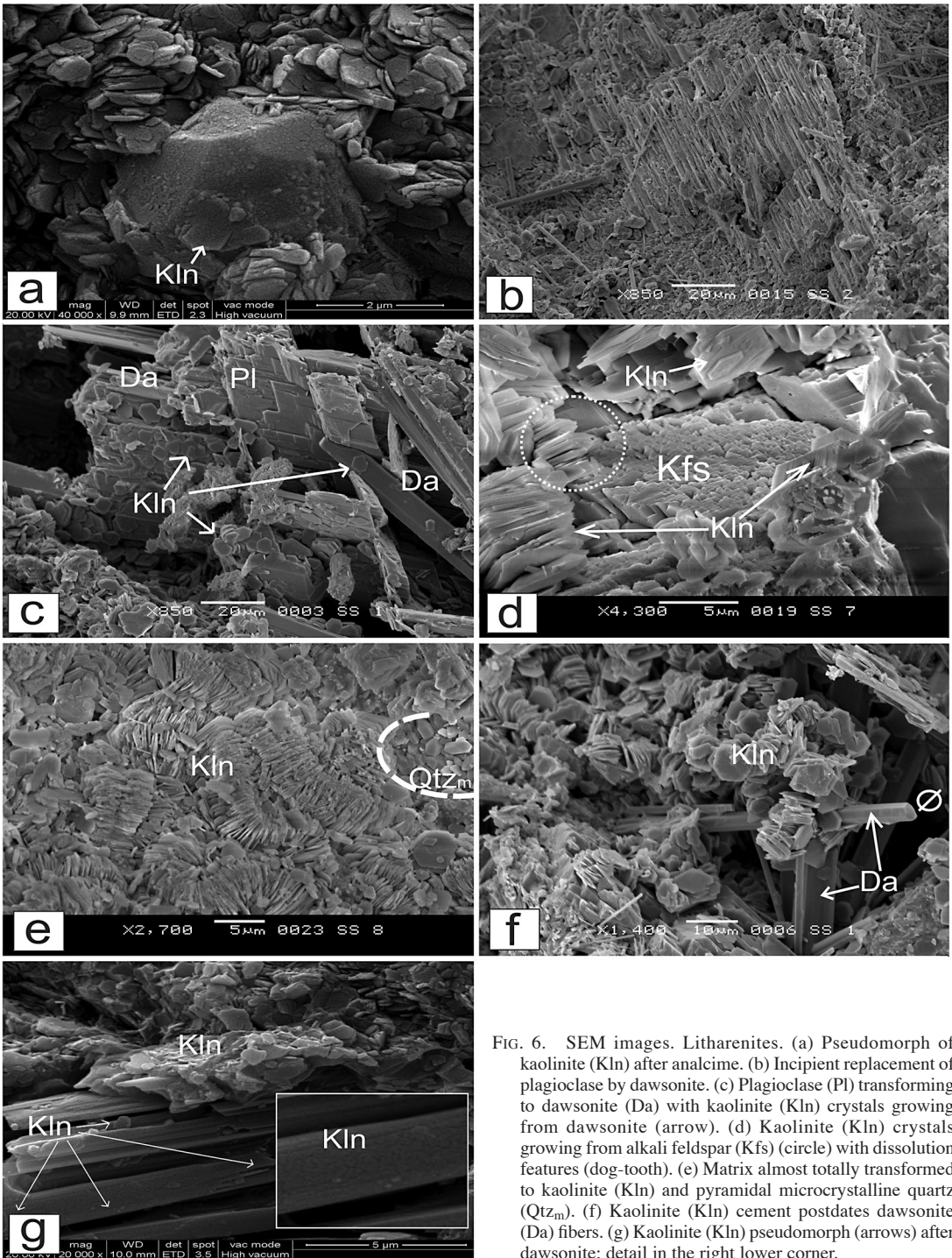
FIG. 6.   SEM images. Litharenites. (a) Pseudomorph of kaolinite (Kln) after analcime. (b) Incipient replacement of plagioclase by dawsonite. (c) Plagioclase (Pl) transforming to dawsonite (Da) with kaolinite (Kln) crystals growing from dawsonite (arrow). (d) Kaolinite (Kln) crystals growing from alkali feldspar (Kfs) (circle) with dissolution features (dog-tooth). (e) Matrix almost totally transformed to kaolinite (Kln) and pyramidal microcrystalline quartz (Qtz_m). (f) Kaolinite (Kln) cement postdates dawsonite (Da) fibers. (g) Kaolinite (Kln) pseudomorph (arrows) after dawsonite; detail in the right lower corner.
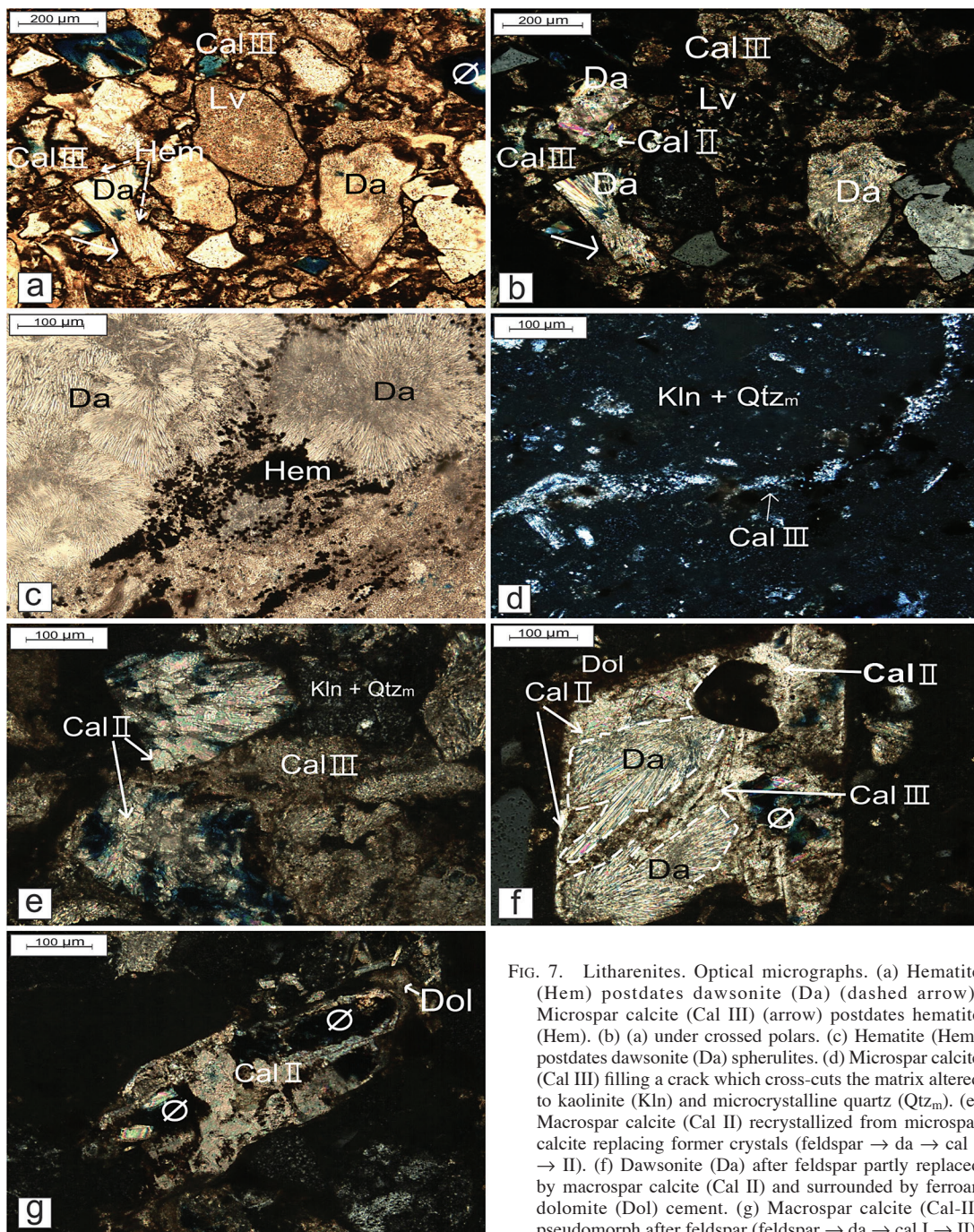
FIG. 7. Litharenites. Optical micrographs. (a) Hematite (Hem) postdates dawsonite (Da) (dashed arrow). Microspar calcite (Cal III) (arrow) postdates hematite (Hem). (b) (a) under crossed polars. (c) Hematite (Hem) postdates dawsonite (Da) spherulites. (d) Microspar calcite (Cal III) filling a crack which cross-cuts the matrix altered to kaolinite (Kln) and microcrystalline quartz (Qtz$_m$). (e) Macrospar calcite (Cal II) recrystallized from microspar calcite replacing former crystals (feldspar → da → cal I → II). (f) Dawsonite (Da) after feldspar partly replaced by macrospar calcite (Cal II) and surrounded by ferroan dolomite (Dol) cement. (g) Macrospar calcite (Cal-II) pseudomorph after feldspar (feldspar → da → cal I → II).
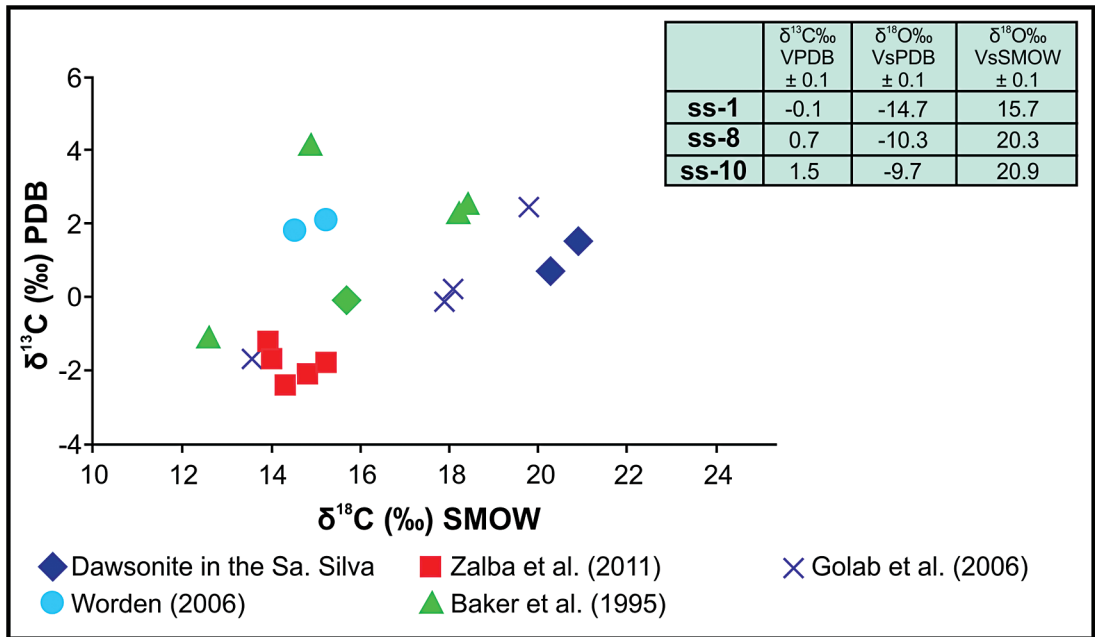
	$\delta^{13}C‰$ VPDB ± 0.1	$\delta^{18}O‰$ VsPDB ± 0.1	$\delta^{18}O‰$ VsSMOW ± 0.1
ss-1	-0.1	-14.7	15.7
ss-8	0.7	-10.3	20.3
ss-10	1.5	-9.7	20.9

FIG. 8. Stable-isotope values for dawsonite-bearing litharenites. Values are also plotted for magmatic CO_2 source taken from the Sydney Basin, Australia (filled triangle), Shabwa Basin in Yemen (filled circle), Upper Hunter region in Australia (cross), and for the Cañadón Asfalto Basin in Argentina (filled square).

DISCUSSION

Paleoenvironment

In the lower and upper sections of the Castillo Formation, isolated fluvial channels with low-to-moderate sinuosity are correlated with those presented in previous works (Paredes 2009, Umazano *et al.* 2012). In addition, Umazano *et al.* (2012) indicated that the deposition of this unit represented a syneruptive period.

In the middle section pyroclastic events were concomitant with the sedimentation in an aggrading subaerial floodplain where shallow lakes were filled with finely laminated ash-fall deposits (Fig. 3g). The predominance of cuspate X and Y-shaped glass shards (Fig. 3f), as well as the absence of angular/blocky shards and welded pumice fragments, would indicate that the eruption which originated these deposits was subaerial in nature, conforming to Fisher & Schmincke (1984b) and Heiken & Wohletz (1985).

As was stated by Surdam (1981) for closed hydrologic systems, the combination of highly reactive pyroclastic material and saline, alkaline solutions in a playa-lake complex is ideal for the crystallization of zeolites. In the middle section, shallow lake deposits of decimeters to a few meters thick and hundreds of meters in lateral extent are interpreted as a playa-lake

complex, as was previously observed for equivalent reservoir units in the subsurface of the basin by Acuña *et al.* (2011).

We suggest a saline, alkaline-lake depositional environment due to the presence of finely laminated ash-fall deposits, which are highly favorable for the formation of zeolites, as was previously stated for volcaniclastic units of the Cerro Barcino Formation, Chubut Group in the Cañadón Asfalto Basin (Iñíguez Rodríguez *et al.* 1987).

Paragenetic sequence

In the litharenites, the feldspar minerals (partially to totally replaced by dawsonite) were not taken into account in the petrographic modal analyses used to study their provenance. The quartz content detected by petrographic analyses is less than the amount of this mineral phase detected by X-ray diffraction techniques (Tables 1, 2). This fact, as well as SEM observation, confirm that most of the quartz, together with the kaolinite, is submicroscopic (Fig. 6e). The amount of submicroscopic quartz points out that it is necessary to consider it as a by-product released to the system in several chemical reactions separated in time and related to different diagenetic processes which involved detrital and authigenic minerals as well. The relative timing of authigenic mineral growth was deduced from

the textural relationships observed in thin sections as well as from SEM images. The proposed paragenetic sequence is summarized in Figure 9.

Compaction put grains in contact with each other. Crushed pumice grains can be observed among the more rigid pyroclastic and volcanic lithic fragments, changing the contacts between grains from straight-straight to concavo-convex ones (Fig. 3d). After mechanical compaction, dawsonite formed *via* dissolution-precipitation (Worden & Burley 2003), the most conspicuous diagenetic replacement process. We interpret that dawsonite is subsequent to mechanical compaction of the host sediments, which normally ends at 70–80 °C (Bjørlykke 1999), because the fibers are not deformed or broken.

Kaolinite and microcrystalline pyramidal quartz postdate dawsonite crystallization because the kaolinite pseudomorphically replaces dawsonite fibers (Fig. 6g) and kaolinite, as a cement, crystallizes over dawsonite fibers (Figs. 6c, f), fills cavities, pores (Figs. 6c, e, f), and cracks. Therefore, there are two kaolinite generations. Hematite cementation occurred after the second kaolinite generation filling cavities, pores, and cracks.

On the crack walls, kaolinite grows as coatings, followed by a central late infilling of hematite.

Euhedral macrospar calcite (II), formed *via* recrystallization of microspar calcite (I), pseudomorphically replaces dawsonite crystals (Fig. 7e) and, in a last step verified in the forward reaction, calcite II partially (Fig. 7f) and totally (Fig. 7g) dissolves dawsonite fibers. Aluminum released during this transformation could have contributed to the formation of a second kaolinite phase. As the amount of calcite in litharenites is not relevant, it is assumed that most of the kaolinite present is the result of the transformation of dawsonite into kaolinite (first generation) plus quartz. In the case of the vitric tuffs, all the kaolinite found could be attributable to the first generation due to the virtual absence of calcite in these rocks.

A third generation of calcite infills fissures and cracks which cross-cut not only the matrix, composed of kaolinite and microcrystalline quartz (Fig. 7d), but also crystals (Fig. 7f), which suggests that calcite III postdates the former association. In addition, ferroan dolomicrite grows around the calcite, which indicates that dolomite is the last carbonate to precipitate (Fig. 7f).

PRODUCTS	MICRO-STRUCTURES	PROCESSES	GEOLOGICAL STAGE	
Volcaniclastic fragments (glass shard-crystalline-lithic)	Lamination (glass shard orientantion)	Deposition	Closed hydrologic basin Fluvial and saline-alkaline lake environments	Eogenesis
		Hydrolyisis		
Loss of porosity	Deformational (concavo-convex contacts)	Mechanical compaction Fluid expulsion (70-80 °C)[a]	Burial diagenesis	Mesogenesis
glass shards→smectite→clinoptilolite → analcime + quartz		Transformation (84-123 °C)[b]		
	Pseudomorphs:	Extension-Compression alkaline-basic hypabyssal bodies intrusion -introduction of CO₂ (100±25 °C)[c]		Telogenesis
analcime → dawsonite + quartz	1. dawsonite after analcime			
feldspars → dawsonite + quartz	2. dawsonite after feldspar		Open hydrologic basin Uplift and erosion	
dawsonite → kaolinite I	3. kaolinite after analcime (via dawsonite)	Introduction of acidic - oxidative meteoric fluids Neoformation Recrystallization Cementation (< 60-70 °C)[d]		
	4. kaolinite after dawsonite			
dawsonite → calcite (I-II) + kaolinite II	5. calcite after dawsonite			
pyrite → hematite	6. hematite after pyrite			
Fe-calcite (III) Fe-dolomite		Passive precipitation		

FIG. 9. Paragenetic sequence. Summary of the diagenetic stages proposed. Reaction (1) taken from Zalba *et al.* (2011). Temperatures taken from: (a) Bjørlykke (1999), (b) Hay (1978), (c) Hellevang *et al.* (2013), (d) Bjørlykke & Jahren (2012).
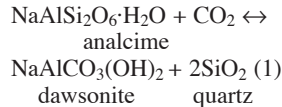
Origin of dawsonite and diagenetic history

Previous studies carried out on other lithostrati-graphic units of the Chubut Group attest to important occurrences of zeolites whose zonal distribution is attributed to burial diagenesis (Iñiguez Rodríguez *et al.* 1987, Manassero *et al.* 2000) and which are summarized in Figure 10, in accordance with the schemes of zeolite zonation of Hay (1978), Surdam & Boles (1979), and Iijima (2001). In addition, in the lower section of the Castillo Formation, sampled at Cerro Chenque (5 km northwest of the dawsonite-bearing stratigraphic profile) plagioclase, alkali feldspars, and analcime are the main components of the volcaniclastic rocks (Fig. 5b), which are characteristic minerals of this unit in other areas of the Golfo San Jorge Basin (Teruggi 1962, Zalba & Andreis 2003, Tunik *et al.* 2004).

We interpret that the zeolite vertical associations described for the Bajo Barreal and Laguna Palacios formations correlate well with the Clinoptilolite-Analcime Zone (<84 °C), while the Castillo Formation correlates with the Analcime Zone (84–123 °C). On the other hand, the presence of analcime-laumontite in the Matasiete Formation would indicate deeper burial diagenesis (>123 °C) for this unit (Fig. 10).

In the study area the fact that analcime is pseudo-morphically replaced by kaolinite (Fig. 6a) implies

that the former was a previous component of these rocks and, moreover, that it is one of the precursors of dawsonite, following the statements of Brobst & Tucker (1974) for the Piceance Creek Basin, USA. The trans-formation of analcime into dawsonite is exemplified by the following reaction (Brobst & Tucker 1974):

$$NaAlSi_2O_6·H_2O + CO_2 \leftrightarrow$$
$$\text{analcime}$$
$$NaAlCO_3(OH)_2 + 2SiO_2 \quad (1)$$
$$\text{dawsonite} \qquad \text{quartz}$$

As analcime is absent in these deposits, the hypothesis that reaction (1) was totally achieved is realistic, so all the analcime was consumed to form dawsonite, and therefore it is not recorded at present. This assumption is also based on Zalba *et al.* (2011) who pointed to the inverse relationship between analcime and dawsonite in volcaniclastic rocks of the Cerro Castaño Member, and considered that analcime was partially transformed to dawsonite.

The stability of dawsonite relative to analcime was studied by mapping the thermodynamic stability of these mineral phases competing for Al at 100, 150, and 200 °C at a fixed CO_2 pressure of 300 bar (Hellevang *et al.* 2011). Assuming that Al is conserved, the authors indicated the dependence of dawsonite stability on CO_2
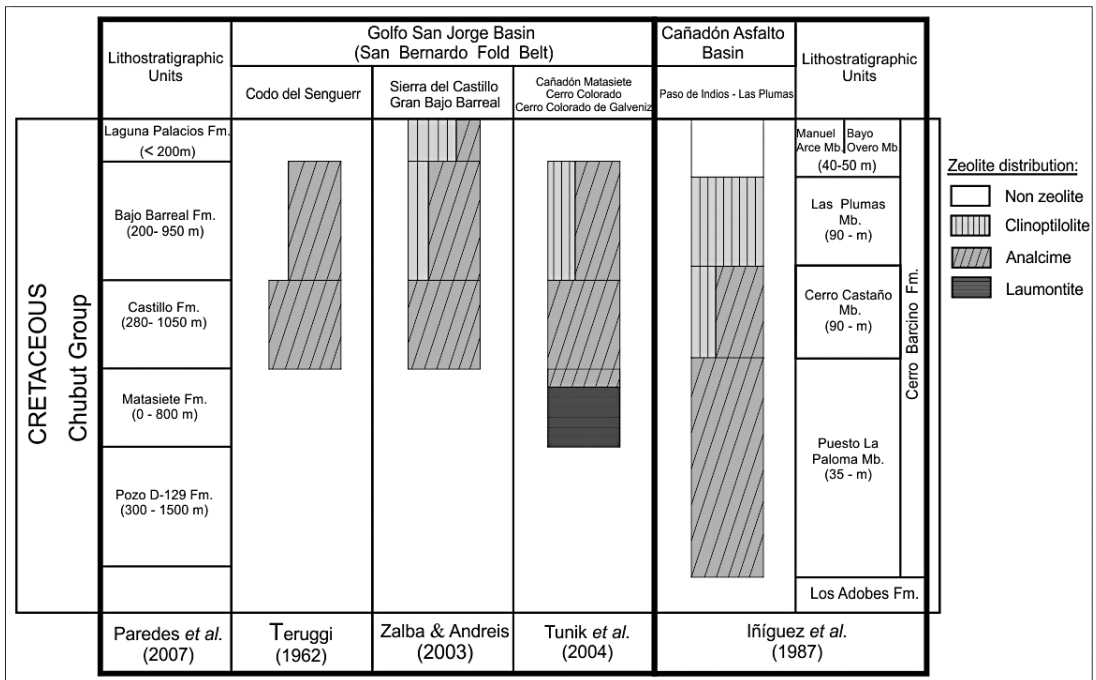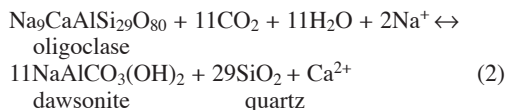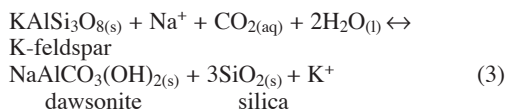

FIG. 10.   Vertical distribution of zeolites in lithostratigraphic units of the Chubut Group. Dawsonite was found in the Cerro Castaño Member (Zalba *et al.* 2011) and in the Castillo Formation (present study).

pressure, and that towards higher temperatures (>150 °C) the analcime stability field increases considerably. In this sense, after the Castillo Formation reached the Analcime Zone (84–123 °C) the injection of CO_2 at relatively high partial pressures could have pushed the unit into the dawsonite stability field at the expense of analcime.

Other dawsonite precursors, as documented by optical microscopy (Fig. 4) and SEM-EDX (Fig. 6c), are plagioclase and the Na-dominant alkali feldspar. The transformation of plagioclase into dawsonite was proposed by Coveney & Kelly (1971):

$$Na_9CaAlSi_{29}O_{80} + 11CO_2 + 11H_2O + 2Na^+ \leftrightarrow$$
    oligoclase
$$11NaAlCO_3(OH)_2 + 29SiO_2 + Ca^{2+} \qquad (2)$$
    dawsonite   quartz

Concerning the transformation of K-feldspar into dawsonite proposed by Bénézeth et al. (2007), represented in equation (3):

$$KAlSi_3O_{8(s)} + Na^+ + CO_{2(aq)} + 2H_2O_{(l)} \leftrightarrow$$
K-feldspar
$$NaAlCO_3(OH)_{2(s)} + 3SiO_{2(s)} + K^+ \qquad (3)$$
    dawsonite   silica

this process has fully been discussed by Hellevang et al. (2011, 2013), who concluded that K-feldspar cannot be a source for Al for dawsonite growth at any temperature. In an isochemically closed system and at temperatures above 120–130 °C, K-feldspar and kaolinite transform into illite, leaving no Al for dawsonite growth (e.g., Hellevang et al. 2011). Moreover, dissolution of K-feldspar at lower temperatures increases the aqueous K^+ activity and prevents further dissolution (Ehrenberg & Nadeau 1989).

However, optical and scanning electron microscopy as well as X-ray diffraction analyses performed for this study provide evidence of the possible transformation of alkali feldspar into dawsonite, based on the following observations: (1) where no dawsonite is present, K-feldspar and plagioclase are important mineral phases (Fig. 5b); and (2) where dawsonite is found, both K-feldspar and plagioclase are depleted (Fig. 5a), moreover in this case no other K-Al mineral phases (muscovite, illite) are present. Therefore, alkali feldspar may have supplied Al and some Na^+ for dawsonite growth, as observed by Worden (2006) for the Lam Formation. As our example seems to have developed in an open system, the K^+ generated could have been removed.

It is assumed that Al and Na were provided not only by internal sources (analcime, plagioclase, and alkali feldspar), but also by external ones derived from basic alkaline subvolcanic bodies. These bodies were intruded into different units of the Chubut Group, including the Castillo Formation, which constitutes the Sarmiento Alkaline Province (Bitschene et al. 1991).

According to Markl & Baumgartner (2002), in alkaline and peralkaline magmatic systems, late-magmatic fluids present strongly basic pH values. The pH of fluids of the $Na_2O–Al_2O_3–SiO_2–H_2O–NaCl$ system mainly depends on the Na/Cl ratio and, to a lesser degree, on salinity and temperature. If the Na/Cl ratio is greater than 1, pH lies between 7 and 12. Under such conditions NaOH is the dominant Na-bearing species and $Al(OH)_4^-$ is the dominant Al-bearing species.

Assuming that Al solubility is a function of pH, when the above physicochemical conditions are achieved, the existence of an external Al source is rational.
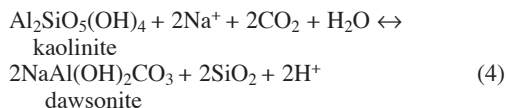
Based on values of $\delta^{13}C$ PDB (–0.1‰ to +1.5‰) obtained from the dawsonite-bearing litharenites, a deep source of CO_2 related to a magmatic origin is presumed, in accordance with tectonically active areas as have been documented in other parts of the world (Baker et al. 1995, Worden 2006, Golab et al. 2006) (Fig. 8). An organic source of CO_2 is considered unlikely because the $\delta^{13}C$ values related to decarbonylation of organic matter are –20‰ and below (Smith et al. 1985). Even though there is a gas generator (Las Heras Group) and source rocks (Pozo D-129 Formation) underlying the Castillo Formation, none of them could have provided the CO_2 because the $\delta^{13}C$ values are not consistent with an organic origin. Also, the lack of marine carbonates in the Castillo Formation, as well as in other units of the Chubut Group, argues against a marine source for the CO_2.

These hypabyssal bodies are associated with conspicuous magmatic activity during the late Eocene-Pleistocene according to Anselmi et al. (2004) and Bruni et al. (2008). Additionally, in the neighboring Cañadón Asfalto Basin, $\delta^{13}C$ values for dawsonite pure crystals (–1.2‰ to –2.4‰) are in accordance with a magmatic origin, related to the presence of hypabyssal alkaline intrusive bodies and correlated to those of the Golfo San Jorge Basin. In light of this evidence, we concur with Zalba et al. (2011) that the dawsonite could not be older than Eocene in age.

The relatively high $\delta^{18}O$ SMOW values for the dawsonite-bearing litharenites, ranging from 15.7 to 20.9, probably represent mineral growth in an aqueous solution with relatively elevated $\delta^{18}O$ and of diagenetic origin, according to values presented by Worden (2006) and Golab et al. (2006) for parental fluids where connate water is the most likely O source.

The absence of dawsonite in vitric tuffs is not related to a textural control, but to its complete replacement by kaolinite.

The transformation of kaolinite into dawsonite was studied by Hellevang et al. (2013) who reported the following equation:

$$Al_2SiO_5(OH)_4 + 2Na^+ + 2CO_2 + H_2O \leftrightarrow$$
    kaolinite
$$2NaAl(OH)_2CO_3 + 2SiO_2 + 2H^+ \qquad (4)$$
    dawsonite

where, if the system is open, with CO_2 and Na^+ supplied, all kaolinite can be converted to dawsonite, and generated H^+ removed. However, from SEM evidence (Fig. 6g and detail) it is clear that kaolinite replaces dawsonite and, therefore, postdates it. It is assumed that the equilibrium for Reaction (4) was shifted to the left. This process represents a further step in the diagenetic story because kaolinite has never been found in the dawsonite-bearing vitric tuffs and litharenites of the Cerro Castaño Member (Zalba *et al*. 2011). The pseudomorphic kaolinite after analcime recognized here (Fig. 6a) would mean that this reaction occurred *via* dawsonite.

From dawsonite formation on, all the diagenetic processes that occurred are related to basin inversion associated with compression, faulting, folding, uplift, erosion, and topographic changes that exposed previously deeply buried sediments to meteoric water influx (see Fig. 9). These phenomena are particularly well developed near basin margins and are reported in the literature as telogenesis (Worden & Burley 2003). Dissolution of feldspars and dawsonite, and precipitation of kaolinite, requires a through flow of meteoric water to remove cations such as Na^+ and K^+ from the host rocks (Bjørlykke 1998). The low solubility of Al at circum-neutral conditions suggests that precipitation of kaolinite requires Al-bearing precursor minerals like dawsonite, as was documented in Figure 6g. Even though dawsonite and kaolinite correlate to a telogenetic stage, they are not associated in time and correspond to different and successive geochemical conditions: low chloride concentration waters that are enriched in Na and HCO_3 and high pCO_2 are necessary for diagenetic dawsonite (Loughnan & Goldbery 1972, Baker *et al*. 1995, Worden 2006); while high fluxes of acidic and low salinity meteoric waters (low K^+/H^+) are required to maintain the pore water in the stability field of kaolinite under telogenetic conditions (Bjørlykke 1998, Worden & Burley 2003).

During Eocene time a generalized magmatic activity in the Golfo San Jorge Basin, associated with basic alkaline subvolcanic intrusions, began with the injection of CO_2. Concomitantly, the dawsonite stability field at the expense of analcime and plagioclase was achieved. During Miocene times a major phase of tectonic inversion in the San Bernardo Fold Belt area occurred (Sylwan *et al*. 2008), promoting fracturing and uplift and the incursion of acidic meteoric-water flux responsible for kaolinite formation.

Conclusions

(1) Dawsonite has been identified in litharenites of the middle and upper sections of the Castillo Formation at Sierra Silva anticline. Its absence in the associated vitric tuffs is not considered to be related to a textural control, but to its complete diagenetic replacement by kaolinite in an open system.

(2) Burial diagenesis transformed silicic zeolites formed in saline alkaline lakes into more alkali ones; accordingly, the Castillo Formation reached the Analcime Zone.

(3) The presumed absence of analcime in the middle and upper sections of the Castillo Formation, considered one of the precursors of dawsonite in volcaniclastic rocks, is due to its complete transformation to dawsonite.

(4) Based on the incomplete transformation of analcime into dawsonite as reported by Zalba *et al*. (2011), which allowed these authors to identify it as one of the precursors of dawsonite, followed by the pseudomorphical transformation of analcime and dawsonite into kaolinite as documented here, we propose that the chemical reaction analcime → kaolinite was complete and achieved *via* dawsonite.

(5) Telogenetic processes, probably beginning in Eocene time, favored the emplacement of basic alkaline hypabyssal bodies (Sarmiento Alkaline Province) which externally sourced Al, Na, and CO_2-fluids at high partial pressure. Replacement of analcime, together with plagioclase and alkali feldspar, occurred, which released Na and Al (internal sources) for the formation of dawsonite. Dawsonite $\delta^{13}C$ PDB (–0.1 to 1.5‰) values are in accordance with deep sources of CO_2 related to a magmatic origin.

(6) As a major phase of tectonic inversion occurred during Miocene time, we interpret that acidic meteoric fluids introduced along faults, fractures, and fissures favored the formation of a first kaolinite phase at the expense of dawsonite. The pseudomorphical replacement of dawsonite by calcite released Al to the system, favoring the formation of a second kaolinite generation. Based on the scarce calcite detected, the hypothesis that most of the kaolinite belongs to the first generation is realistic. Passive precipitation of hematite, calcite, and dolomite occurred as a final event.

References

Acuña, C., Schiuma, A., Parra, D., Droeven, C., Bernedo, M., & Paredes, J. (2011) Modelo paleoambiental de la Formación Mina del Carmen en el yacimiento Cerro Dragón, Cuenca del Golfo San Jorge, Argentina. Trabajos Técnicos. *Actas VIII Congreso de Exploración y Desarrollo de Hidrocarburos (Mar del Plata)*, 419–442.

Anselmi, G., Gamba, M.T., & Panza, J.L. (2004) Hoja Geológica 4369-IV, Los Altares, Provincia del Chubut. *Instituto de Geología y Recursos Minerales, Servicio Geológico Minero Argentino, Boletín* **312**, 1–98.

Baker, J.C., Bai, G.P., Hamilton, P.J., Golding, S.D., & Keene, J.B. (1995) Continental-scale magmatic carbon dioxide seepage recorded by dawsonite in the Bowen–Gunnedah–Sydney Basin system, eastern Australia. *Journal of Sedimentary Research* **A65**, 522–530.

Barcat, C., Cortiñas, J.S., Nevistic, V.A., & Zucchi, H.E. (1989) Cuenca Golfo San Jorge. *In* Cuencas Sedimentarias Argentinas (G. Chebli & L.A. Spalletti, eds.). *Instituto Superior de Correlación Geológica, Universidad Nacional de Tucumán, Serie de Correlación Geológica* **6**, 319–345.

Bénézeth, P., Palmer, D.A., Anovitz, L.M., & Horita, J. (2007) Dawsonite synthesis and reevaluation of its thermodynamic properties from solubility measurements: Implications for mineral trapping of CO₂. *Geochimica et Cosmochimica Acta* **71**, 4438–4455.

Bérar, J.F. & Lelann, P. (1991) E.S.D.'s estimated probable error obtained in Rietveld refinements with local correlations. *Journal of applied crystallography* **24**, 1–5.

Bish, D.L. & Post, J.E. (1993) Quantitative mineralogical analysis using Rietveld full-pattern fitting method. *American Mineralogist* **78**, 932–940.

Bitschene, P.R., Giacosa, R., & Marquez, M. (1991) Geologic and mineralogical aspects of the Sarmiento Alkaline Province in Central Eastern Patagonia, Argentina. *Actas VI Congreso Geológico Chileno*, 328–331.

Bjørlykke, K. (1998) Clay mineral diagenesis in sedimentary basins—a key to the prediction of rock properties. Examples from the North Sea Basin. *Clay minerals* **33**, 15–34.

Bjørlykke, K. (1999) Principal aspects of compaction and fluid flow in mudstones. *In* Mud and mudstones: Physical and fluid-flow properties (A.C. Aplin, A.J. Fleet, & J.H.S. Macquaker, eds.). *Geological Society of London Special Publication* **158**, 73–78.

Bjørlykke, K. & Jahren, J. (2012) Open or closed geochemical systems during diagenesis in sedimentary basins: Constraints on mass transfer during diagenesis and the prediction of porosity in sandstone and carbonate reservoirs. *American Association of Petroleum Geologists Bulletin* **96**, 2193–2214.

Bridge, J.S., Jalfin, G.A., & Georgieff, S.M. (2000) Geometry, lithofacies, and spatial distribution of Cretaceous fluvial sandstone bodies, San Jorge Basin, Argentina: Outcrop analog for the hydrocarbon-bearing Chubut Group. *Journal of Sedimentary Research* **70**, 341–359.

Brobst, D.A. & Tucker, J.D. (1974) Composition and relation of analcime to diagenetic dawsonite in oil shale and tuff in the Green River Formation, Piceance Creek basin, northwestern Colorado. *Journal of Research of the U.S. Geological Survey* **2**, 35–39.

Bruni, S., D'Orazio, M., Haller, M., Innocenti, F., Manetti, P., Pécskay, Z., & Tonarini, S. (2008) Time-evolution of magma sources in a continental back-arc setting: the Cenozoic basalts from Sierra de San Bernardo, Patagonia, Chubut, Argentina. *Geological Magazine* **145(5)**, 714–732.

Cladera, G., Limarino, C.O., Alonso, M.S., & Rauhut, O.W.M. (2004) Controles estratigráficos en la preservación de restos de vertebrados en la Formación Cerro Barcino (Cenomaniano), Provincia del Chubut. *Revista de la Asociación Argentina de Sedimentología* **11(2)**, 39–56.

Coplen, T.B. (1994) Reporting of stable hydrogen, carbon, and oxygen isotopes abundances. *Pure Applied Chemistry* **66**, 273–276.

Coveney, R.M. & Kelly, W.C. (1971) Dawsonite as a daughter mineral in hydrothermal fluid inclusions. C*ontributions to Mineralogy and Petrology* **32**, 334–342.

Dickson, J.A.D. (1965) A modified technique for carbonates in thin section. *Nature* **205**, 587.

Ehrenberg, S.N. & Nadeau, P.H. (1989) Formation of diagenetic illite in sandstones of the Garn Formation, Haltenbanken area, Mid-Norwegian Continental shelf. *Clay Minerals* **24**, 233–253.

Fernández Gianotti, J.R. (1969) La diabasa de Muzeca y su contenido de niquel, Sierra de San Bernardo, Provincia del Chubut, República Argentina. *Revista de la Asociación Geológica Argentina* **24(3)**, 159–171.

Ferrini, V., Martarelli, L., De Vito, C., Cina, A., & Deba, T. (2003) The Koman dawsonite and realgar-orpiment deposit, northern Albania: inferences on processes of formation. *Canadian Mineralogist* **41**, 413–427.

Fisher, R.V. & Schmincke, H.U. (1984a) *Pyroclastic Rocks*. Springer-Verlag, Berlin, Germany.

Fisher, R.V. & Schmincke, H.U. (1984b) Volcaniclastic sediment transport and deposition. *In* Sediment Transport and Depositional Processes (K. Pye, ed.). Blackwell Scientific Publications, Oxford, United Kingdom (351–388).

Fitzgerald, M.G., Mitchum, R.M., Jr, Uliana, M.A., & Biddle, K.T. (1990) Evolution of the San Jorge Basin, Argentina. *The American Association of Petroleum Geologists* **74**, 879–920.

Folk, R.L., Andrews, P.B., & Lewis, D.W. (1970) Detrital sedimentary rock classification and nomenclature for use

in New Zealand. *New Zealand journal of Geology Geophysics* **13**, 937–968.

GENISE, J.F., SCIUTTO, J.C., LAZA, J.H., GONZALEZ, M.G., & BELLOSI, E.S. (2002) Fossil bee nests, coleopteral pupal chambers and tuffaceous paleosols from the Late Cretaceous Laguna Palacios Formation, Central Patagonia (Argentina). *Palaeogeography, Palaeoclimatology, Palaeoecology* **177**, 215–235.

GILLESPIE, M.R. & STYLES, M.T. (1999) BGS Rock Classification Scheme - Volume 1. Classification of igneous rocks. British Geological Survey Research Reports (2nd. Edition). RR99-06, Nottingham. <http://www.bgs.ac.uk/bgsrcs/ home.html>

GOLAB, A.N., CARR, P.F., & PALAMARA, D.R. (2006) Influence of localised igneous activity on cleat dawsonite formation in Late Permian coal measures, Upper Hunter Valley, Australia. *International Journal of Coal Geology* **66(4)**, 296–304.

GOLDBERY, R. & LOUGHNAN, F.C. (1977) Dawsonite, alumohydrocalcite, nordstrandite and gorceixite in Permian marine strata of the Sydney Basin, Australia. *Sedimentology* **24**, 565–579.

HAY, R.L. (1963) Zeolitic weathering in Olduvai Gorge, Tanganyika. *Geological Society of American Bulletin* **74**, 1281–1286.

HAY, R.L. (1964) Phillipsite of saline lakes and soils. *American Mineralogist* **49**, 1366–1387.

HAY, R.L. (1978) Geologic occurrence of zeolites. *In* Natural zeolites: occurrence, properties, use (L.V. Sand & F.A. Mumpton, eds.). Pergamon Press, Elmsford, New York, United States (135–143).

HECHEM, J.J., HOMOVC, J.F., & FIGARI, E.G. (1990) Estratigrafía del Chubutiano en las Sierras de San Bernardo, Cuenca del Golfo San Jorge, Chubut, Argentina. *Actas XI Congreso Geológico Argentino (San Juan)* **2**, 173–176.

HEIKEN, G. & WOHLETZ, K. (1985) *Volcanic Ash*. University of California Press, Berkeley, United States.

HELLEVANG, H., DECLERCQ, J., & AAGAARD, P. (2011) Why is dawsonite absent in CO_2 charged reservoirs? *Oil & Gas Science and Technology, Revue d'IFP Energies nouvelles* **66**, 119–135.

HELLEVANG, H., AAGAARD, P., & JAHREN, J. (2013) Will dawsonite form during CO_2 storage? *Greenhouse gas: Science and Technology*, 1–9, DOI: 10.1002/ghg.

IIJIMA, A. (2001) Zeolites in Petroleum and Natural Gas Reservoirs. *In* Natural zeolites: occurrence, properties, applications (D.L. Bish & D.W. Ming, eds.). *Reviews in Mineralogy and Geochemistry* **45**, 347–402.

IÑÍGUEZ RODRÍGUEZ, A.M., ZALBA, P.E., & MAGGI, J.H. (1987) Clinoptilolita y analcima en miembros del Grupo Chubut, entre Paso de Indios y Las Plumas, Provincia de Chubut, Argentina. *Actas X Congreso Geológico Argentino (Tucumán)* **1**, 75–78.

LESTA, P.J. & FERELLO, R. (1972) Región Extraandina de Chubut y Norte de Santa Cruz. *In* Geología Regional Argentina (A.F. Leanza, ed.). Academia Nacional de Ciencias de Córdoba, Córdoba, Argentina (601–653).

LIU, N., LIU, L., QU, X., YANG, H., WANG, L., & ZHAO, S. (2011) Genesis of authigene carbonate minerals in the Upper Cretaceous reservoir, Honggang Anticline, Songliao Basin: A natural analog for mineral trapping of natural CO_2 storage. *Sedimentary Geology* **237**, 166–178.

LOUGHNAN, F.C. & GOLDBERY, R. (1972) Dawsonite and analcite in the Singleton Coal Measures of the Sydney Basin. *American Mineralogist* **57**, 1437–1447.

MANASSERO, M., ZALBA, P.E., ANDREIS, R.R., & MOROSI, M. (2000) Petrology of continental pyroclastic and epiclastic sequences in the Chubut Group (Cretaceous): Los Altares-Las Plumas area, Chubut, Patagonia, Argentina. *Revista Geológica de Chile* **27**, 13–26.

MARKL, G. & BAUMGARTNER, L. (2002) pH changes in peralkaline late-magmatic fluids. *Contributions to Mineralogy and Petrology* **144**, 331–346.

MASON, G.M. (1983) Mineralogy of the Mahogany Marker Tuff of the Green River Formation, Piceance Creek Basin, Colorado. *In* Proceedings of the Sixteenth Oil Shale Symposium (J.H. Gary, ed.). Colorado School of Mines, Golden, Colorado, United States (124–131).

MCCREA, J.M. (1950) On the isotopic chemistry of carbonates and a paleotemperature scale. *Journal of Chemical Physics* **18**, 849–857.

MENEGATTI, N., MASSAFERRO, G., FERNÁNDEZ, M., & GIACOSA, R. (2013) Petrología de los cuerpos básicos alcalinos al sur de Chubut. *Actas II Simposio de Petrología Ígnea y Metalogénesis Asociada*, 66.

PAREDES, J.M. (2009) Sedimentary Evolution of the Golfo San Jorge Basin, Central Patagonia, Argentina. *In* Argentinean Fluvial Basins: Ancient and present day examples (L.M. Ibañez, M.S. Moyan, & Aceñolaza G.F., eds.). *Excursion Guide Book, IX International Conference on Fluvial Sedimentology, Basin Analysis Series I*, Facultad de Ciencias Naturales e Instituto Miguel Lillo de la Universidad Nacional de Tucumán, (187–275).

PAREDES, J.M., FOIX, N., COLOMBO, F., NILLNI, A., ALLARD, J.O., & MARQUILLAS, R. (2007) Volcanic and climatic control on fluvial style in a high-energy system: the Lower Cretaceous Matasiete Formation, Golfo San Jorge basin, Argentina. *Sedimentary Geology* **202**, 96–123.

PETTIJOHN, F.J., POTTER, P.E., & SIEVER, R. (1987) *Sand and Sandstone*. Springer Verlag, New York, N.Y, 553 pp.

RIETVELD, H.M. (1969) A profile refinement method for nuclear and magnetic structures. *Journal of Applied Crystallography* **2**, 65–71.

Rodríguez Carvajal, J. (2001) Recent development of the Program FULLPROF. *Commission on Powder Diffraction (IUCr), Newsletter* **26**, 12–19.

Sciutto, J.C. (1981) Geología del codo del Río Senguerr, Chubut, Argentina. *Actas VIII Congreso Geológico Argentino (San Luis)* **3**, 203–219.

Smith, J.W. & Milton, C. (1966) Dawsonite in the Green River Formation of Colorado. *Economic Geology* **61**, 1029–1042.

Smith, J.W., Gould, K.W., Hart, G.H., & Rigby, D. (1985) Isotopic studies of Australian natural and coal seam gases. *Bulletin of the Australasian Institute of Mining and Metallurgy* **290**, 43–51.

Stevenson, J.S. & Stevenson, L.S. (1977) Dawsonite-fluorite relationships at Montreal-area localities. *Canadian Mineralogist* **15**, 117–120.

Stevenson, J.S. & Stevenson, L.S. (1978) Contrasting dawsonite occurrences from Mont St-Bruno, Quebec. *Canadian Mineralogist* **16**, 471–474.

Surdam, R.C. (1981) Zeolites in closed hydrologic systems. *In* Mineralogy and Geology of Natural Zeolites (F.A. Mumpton, ed.). *Reviews in Mineralogy* **4**, 65–91.

Surdam, R.C. & Boles, J.R. (1979) Diagenesis of volcaniclastic sandstones. *In* Aspects of Diagenesis (P.A. Scholle & P.R. Schluger, eds.). *Society of Economic Paleontologists and Mineralogists, Special Publication* **26**, 227–242.

Sylwan, C.A., Rodríguez, J.F., & Strelkov, E.E. (2008) Petroleum system of the Golfo the San Jorge Basin, Argentina. *In* Sistemas petroleros de las cuencas andinas (C.E. Cruz, J.F. Rodríguez, J.J. Hechem, & H.J. Villar, eds.). VII Congreso de Exploración y Desarrollo de Hidrocarburos, Simposio de Sistemas Petroleros de las Cuencas Andinas (53–77).

Teruggi, M.E. (1962) Sobre la presencia de analcima sedimentaria en el chubutiano del Codo del Senguerr. *Revista del Museo de La Plata (Nueva serie) Sección geología* **5**, 193–217.

Teruggi, M.E. & Rosetto, H. (1963) Petrografía del chubutiano del Codo del Senguerr. *Boletín de Informaciones Petroleras* **354**, 18–35.

Tunik, M.A., Vietto, M.E., Sciutto, J.C., & Estrada, E. (2004) Procedencia de areniscas del Grupo Chubut en el área central de la Sierra de San Bernardo. Análisis preliminar. *Revista de la Asociación Geológica Argentina* **59**, 601–606.

Umazano, A.M., Bellosi, E., Visconti, G., & Melchor, R.N. (2008) Mechanism of aggradation in fluvial systems influenced by explosive volcanism: An example from the Upper Cretaceous Bajo Barreal Formation, San Jorge Basin, Argentina. *Sedimentary Geology* **203**, 213–228.

Umazano, A.M., Bellosi, E., Visconti, G., & Melchor, R.N. (2012) Detecting allocyclic signals in volcaniclastic fluvial successions: Facies, architecture and stacking pattern from the Cretaceous of central Patagonia, Argentina. *Journal of South American Earth Sciences* **40**, 94–115.

Worden, R.H. (2006) Dawsonite cement in the Triassic Lam Formation, Shabwa Basin, Yemen: a natural analogue for a potential mineral product of subsurface CO$_2$ storage for greenhouse gas reduction. *Marine and Petroleum Geology* **23**, 61–77.

Worden, R.H. & Burley, S.D. (2003) Sandstone Diagenesis: the evolution of sand to stone. *In* Sandstone Diagenesis: Recent and Ancient (S.D. Burley & R.H. Worden, eds.). International Association of Sedimentologists, Blackwell Publishing, Reprint Series 4, Oxford, United Kingdom (3–44).

Zalba, P.E. & Andreis, R.R. (2003) Procesos diagenéticos en el Grupo Chubut: Formaciones Castillo, Bajo Barreal y Laguna Palacios (Albiano-Maastrichtiano), Patagonia, Chubut, Argentina. *III Congreso Mexicano de zeolitas naturales*, 91–93.

Zalba, P.E., Conconi, M.S., Morosi, M., Manassero, M., & Comerio, M. (2011) Dawsonite in tuffs and litharenites of the Cerro Castaño Member, Cerro Barcino Formation, Chubut Group (Cenomanian), Los Altares, Patagonia, Argentina. *Canadian Mineralogist* **49**, 503–520.